Technical Report No. 32-688

Design for a Space Molecular Sink Simulator

J. B. Stephens

D. A. Wallace

JET PROPULSION LABORATORY

CALIFORNIA INSTITUTE OF TECHNOLOGY

PASADENA, CALIFORNIA

November 15, 1964

Technical Report No. 32-688

Design for a Space Molecular Sink Simulator

J. B. Stephens
D. A. Wallace

R. E. Covey

R. E. Covey, *Chief*
Space Simulators and Facility
Engineering Section

JET PROPULSION LABORATORY
CALIFORNIA INSTITUTE OF TECHNOLOGY
PASADENA, CALIFORNIA

November 15, 1964

CONTENTS

CONTENTS (Cont'd)

FIGURES

PREFACE

The design described in this Report is the result of a design contract with the Celestial Research Corporation, sponsored by the Jet Propulsion Laboratory. One of the authors, D. A. Wallace, is a senior research engineer with the Celestial Research Corporation and was assisted by K. W. Rogers.

ABSTRACT

The results of a design study for a space molecular sink vacuum system facility are presented. The sharp-V-grooved, LN_2-cooled, molecular trap shrouds are a capture improvement of an order of magnitude over smooth walls and capture 99.96% of the condensable molecules emanating from the test item before they can return. A non-flaking, Dewar-fed, 20°K helium cryopump is used to remove all gases non-condensable at 77°K except helium and hydrogen. Ion pumps operating at 77°K, in conjunction with titanium sublimation onto the molecular trap shrouds, remove the two remaining gases. A 270-cfm pump (operating in the viscous-flow regime) and a 140 liter/sec turbo-molecular impact pump are used to rough-pump the double-walled, double-doored, bottom-loading vacuum chamber, 10 feet in diameter, and to sustain the guard vacuum. The chamber is decontaminated and titanium evaporant is removed by 250°C vacuum bake-out in conjunction with glass-bead blasting. Contaminant-free loading, pump-down, sustained ultra-high-vacuum operation, back-fill, and unloading techniques are described. Conventional ultra-high-vacuum and cryogenic instrumentation and controls are used. Cryogenic quartz-crystal microbalances are used to measure contaminant migration.

I. INTRODUCTION

During flight through space, a considerable molecular flux emanates from various parts of the spacecraft. Some of this flux impinges upon surfaces of the spacecraft and deposits upon them as contaminants; the remainder leaves the vehicle and does not return. Various parts of the spacecraft, particularly scientific instruments of an optical nature, are adversely affected by this contamination.

In addition, many of the active environments of space (particle and radiation fluxes) produce marked effects upon the surfaces of spacecraft components. The action of these fluxes upon the surfaces is dependent upon the gases being removed by the permissive molecular sink once they are dislodged from the surface.

A need has thus arisen for a space molecular sink simulator in which spacecraft self-contamination and surface-effect problems can be investigated.

The objective of the space molecular sink project is the creation of a permissive vacuum environment around a space component in the laboratory so as to simulate as closely as possible the condition in space under which molecules leaving the immediate neighborhood of a spacecraft have essentially zero probability of returning to it.

II. MOLSINK FEATURES

A. Requirements

The requirements for a molecular sink simulation facility, and the way in which the MOLSINK meets these requirements, are as follows:

Molecular Sink. The MOLSINK system is designed to capture all but 4 of every 10,000 condensable molecules emanating from a 10-in.-diameter test item before they can return.

Clean Pumps. The pumping techniques used in the MOLSINK system are inherently contaminant-free.

Clean Chamber. The design allows the chamber to be decontaminated by the use of glass-bead blasting, followed with vacuum baking.

Clean Operation. Loading, pump-down, steady-state operation, backfill, and unloading can all be accomplished without contaminants migrating back to the test item.

Flexibility. The system has been designed so that each basic subsystem is a discrete entity. This feature enables new or improved elements to be used, thus reducing the possibility of early obsolescence.

Size. The chamber is large enough to test real spacecraft components, yet does not require field erection and will fit within an existing building.

Expandable Techniques. The design incorporates only those techniques of fabrication, assembly, operation, and decontamination that can be applied to larger second-generation facilities.

B. Brief Description

The MOLSINK system (see Figs. 1 and 2) is designed to use sharp-V-grooved, LN_2-cooled, moltrap shrouds to effect a molecular sink. These shroud elements are suspended inside a double-walled, double-doored vacuum chamber 10 ft in diameter. The inner liner and inner door are also cooled with LN_2.

Liquid-helium cryopumps, in conjunction with sub-pumps and ion pumps, are used to sustain ultra-high vacuums in the test volume after the inner door is closed. A mechanical pump, in conjunction with a turbomol pump, is used to rough-pump the chamber and to sustain the guard vacuum.

Nichrome ribbon heaters mounted between the moltrap elements and the inner liner supply bake-out heat.

Cryogenic quartz-crystal microbalances are used to monitor the condensable molecular flux within the chamber. Nude ion gauges and residual gas analyzers supply information about the indigenous gases.

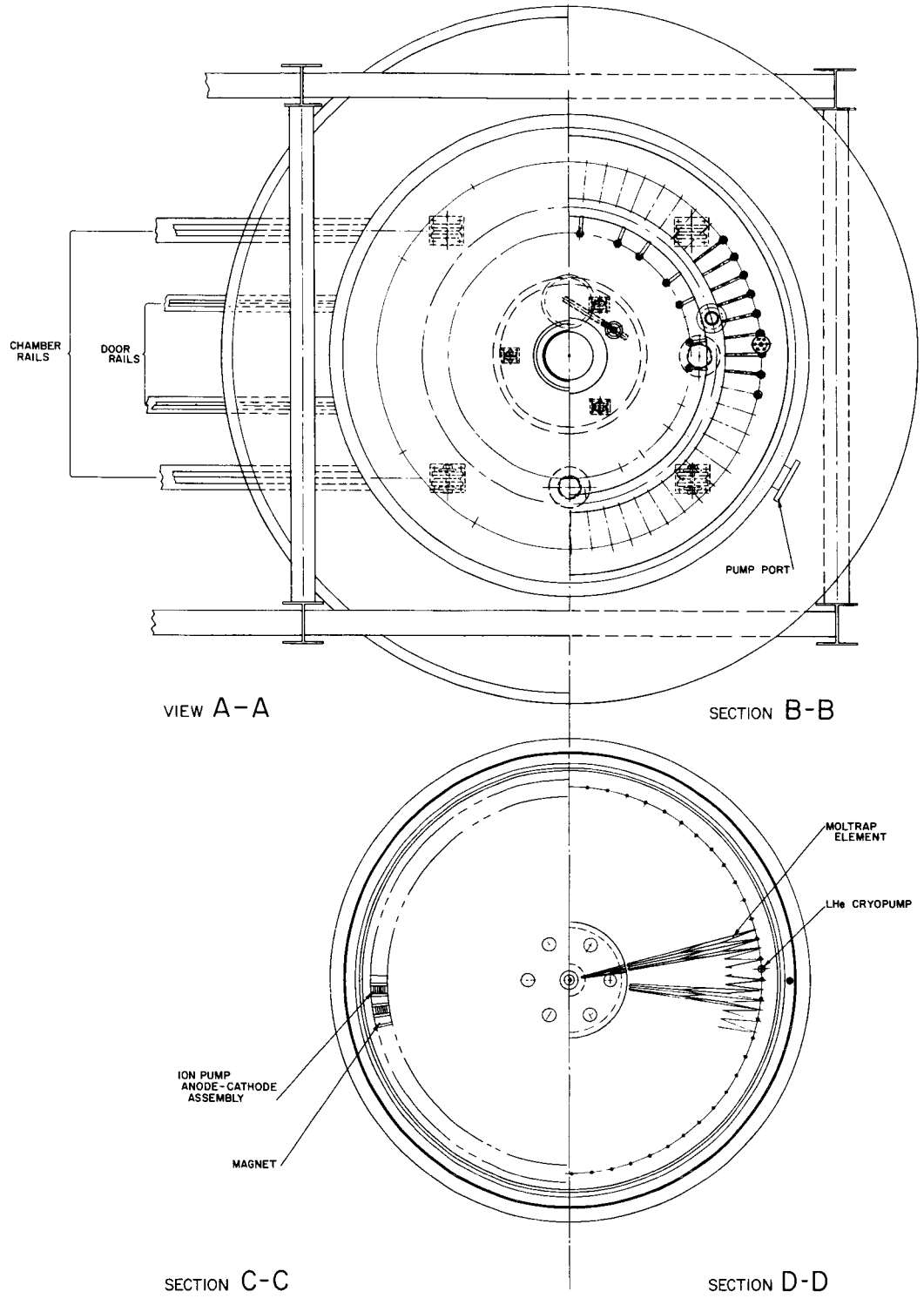

Fig. 1. MOLSINK plan view

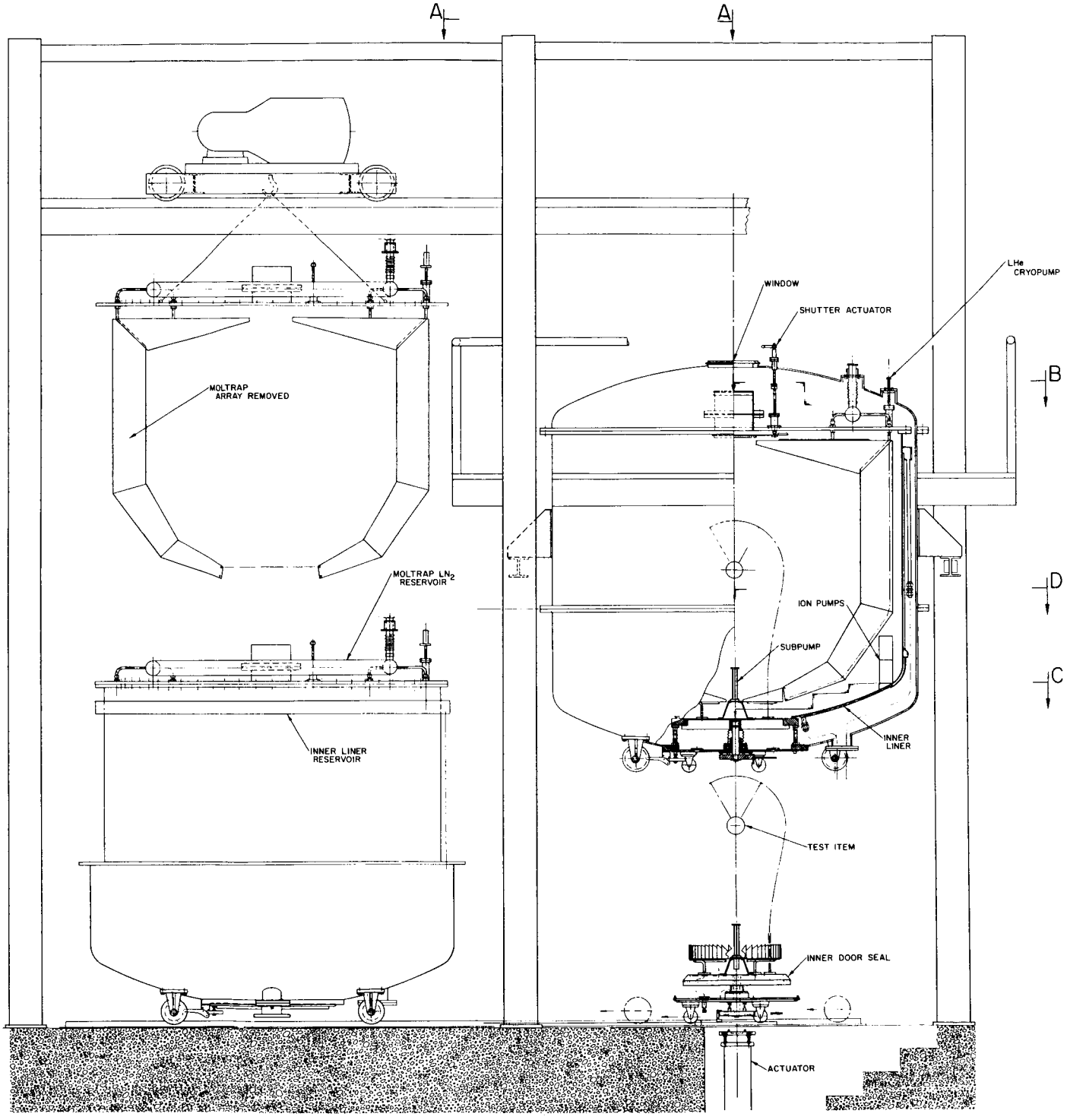

Fig. 2. MOLSINK elevation view

III. MOLSINK DESIGN

A. Basic Approach

The mean free path of a molecule in space is practically infinite (probably of the order of 10^5 km); in a space-vacuum simulation chamber it is no greater than the largest dimensions of the chamber. Molecules generated by the test article collide with and reflect from the chamber walls unless the chamber walls act as sinks for the molecules. Most engineering surfaces, regardless of temperature, do not provide a unity capture probability for gas molecules. Further, it is not clearly understood how the microscopic structure of a solid surface relates to the capture probability. It is known empirically that certain substances, such as charcoal and sputtered titanium, when kept at cryogenic temperatures, do afford high capture probabilities, but these have fairly low saturation limits. It is also known that appropriately arranged macroscopic surfaces act as black bodies in electromagnetic radiation, and the analogy between black-body radiation and molecular flux is well established.

The quest for the perfect sink for molecules can thus follow two routes: to understand and thereafter to construct microscopic surface structures to produce and maintain unity capture probability, or to devise macroscopic arrays that yield near-unity equivalent capture probabilities. The former approach, while scientifically challenging, clearly represents a long and tedious task, while the latter, being based on well-established principles, is relatively easy to pursue.

B. Molecular Sink Analysis

There are two basic types of surface arrays that could be considered for the MOLSINK arrays. These two, which will be named the wedge-fin type and the radial-fin type, differ in the directional distribution of returned molecules. When a molecule impinges on a surface and, after certain exchanges of energy and momentum with the surface, reflects from it, the direction at which it departs is generally random, regardless of the incidence angle. This means that from the point of impact the molecule may be reflected in any direction within the hemisphere over the point. In any cross-sectional plane, normal to the reflecting surface, the distribution of molecular flux with respect to direction, under the above-mentioned diffuse reflection condition, is as shown in the sketch below, wherein the magnitude of the vector represents the flux density.

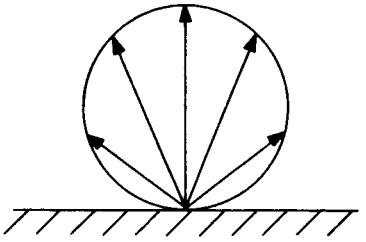

A wedge-fin-type array, because of a uniform flux distribution, results in diffuse reflection of molecules, the integrated (over-all directions) flux of which is some fraction of the incident flux, the fraction depending on the angle of the wedge and on the capture probability of the wedge surface (see sketch below). It can be shown that the array capture coefficient in this case is proportional to L/W.

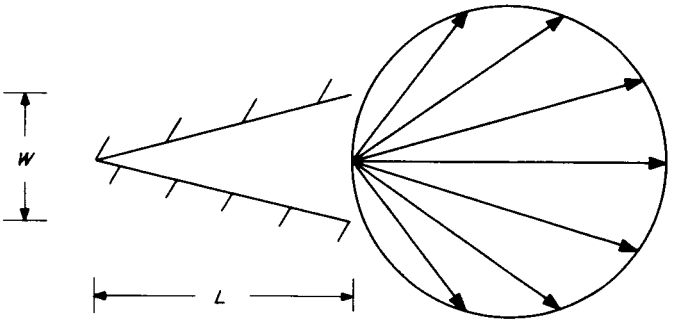

A radial-fin-type array, which has very nearly parallel sides and a bottom normal to the sides, as shown below, produces a nondiffuse reflected flux of molecules. This type of array has an array capture coefficient that is proportional to L^2/W.

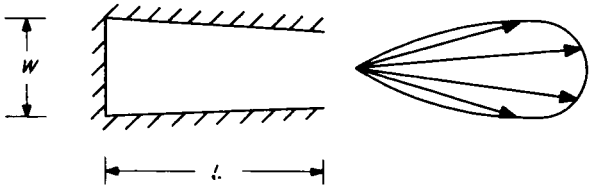

While the total reflected flux is smaller for the radial-fin type than for the wedge-fin type, for the same W and L, the former flux is concentrated in directions closely grouped around the axis of the tube. Thus, if a chamber is surrounded with arrays, the wedge-fin type would result in diffusely distributed returning molecules, while

the radial-fin type would "focus" the returning molecules at the centered source. In fact, it is readily shown that the total rate at which returning molecules arrive at a centered source is the same for a radial-fin-type array as for a smooth spherical shell. However, the total number of returning molecules present in the chamber can be considerably lower for the case of the radial-fin array than for either a smooth sphere or a wedge-fin-type array.

For the design of the MOLSINK, in which there is to be a centered source onto which the self-contamination from returning molecules is to be held below a specified amount, the wedge-fin-type array can be shown to be generally more advantageous than the radial-fin type.

C. Analysis of Wedge-Fin Array

A moltrap array of the wedge-fin type (shown in the sketch below) can be analyzed using the following

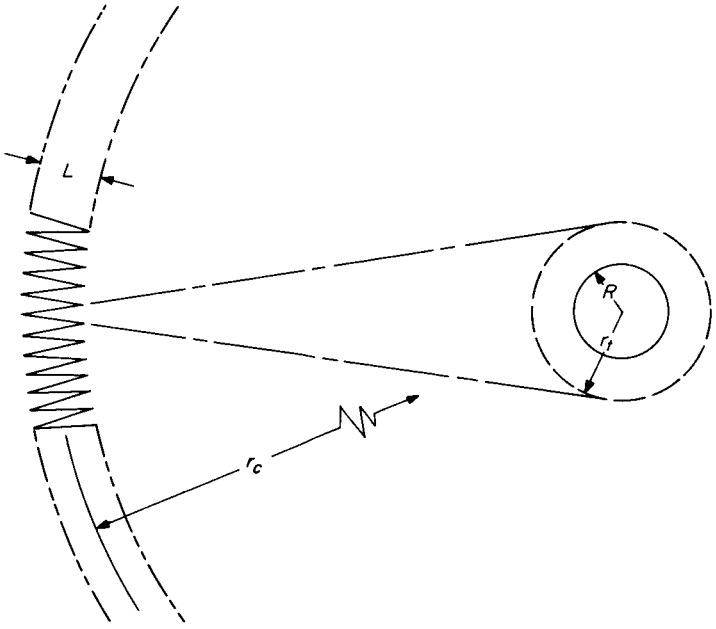

equations

$$\Gamma = \frac{N_r}{N_s} = \left(\frac{R}{r_c}\right)^2 (1 - \sigma) \frac{r_t}{r_c} \qquad (1)$$

or

$$\Gamma = \frac{N_r}{N_s} = \left(\frac{R}{r_c}\right)^2 (1 - \sigma) \cos \eta_0 \qquad (2)$$

provided some simplifying assumptions are made:

1. All molecules emanating from the test item have a surface capture coefficient of σ on the array surfaces.
2. The test item is spherical and emits molecules uniformly as to temperature and direction.
3. The molecular trap array is spherical and has an effective radius of r_c.
4. There are no blunt surfaces. That is, the wedges have perfectly sharp edges and roots.
5. The wedge fins have negligible depth as compared with the array radius.
6. The radius of the sphere to which the fin surfaces are tangent is equal to or larger than the test item radius.
7. The molecules rebound diffusely from the array surfaces, i.e., with a cosine spatial distribution.
8. The molecules that rebound and do not strike the test item do not rebound again.

The derivations of Eqs. (1) and (2) are performed in Appendixes A, B, and C. The error involved in making the above stated assumptions is analyzed in Appendixes D through I.

If σ is assumed to be 0.80 (400°K H_2O vapor on 77°K surface, Ref. 1), if R and r_t both equal 5 in. and r_c equals 43 in., then from Eq. (1), Γ is 3.16×10^{-4}. The ratio of returning to emitted molecules for the actual design, incorporating the effects of having a cylindrical array, blunt surfaces, array gaps, significant fin depth, and multiple wall collisions, as calculated in the Appendixes, would be 3.89×10^{-4}.

D. Design of Wedge-Fin Array

The optimum array design requires the smallest possible surface angle with negligible normal edge area. The ideal solution probably requires the use of very thin folded foil or sharp machined serrations in a solid plate. Since both solutions are development programs, the engineering effort has been to find the maximum molecular trap ratio attainable with standard established fabrication techniques. A molecular trap ratio near 10:1 has been found to be the maximum ratio economically attainable

at this time. Two approaches have been examined in detail, one using folded sheets and one using extrusion.

1. Folded Sheet Construction

One hundred and twenty folded 0.020-in. copper-sheet fin-array elements, 10 in. deep, each cooled by a ½-in. copper tube furnace-brazed in the fold, are gravity-fed LN_2 and are suspended from special bulkhead fittings in the top plate of the inner liner. This configuration provides a 10:1 molecular trap ratio with only 9½% increase in the recontamination coefficient due to the blunt edge effects.

2. Extrusion Construction

Extruded aluminum sections with molecular trap ratios of 8:1 are attainable with acceptable root and fin-tip radii. Their excessive weight and their requirements for fin-tip machining and aluminum welding cause this approach to be the second choice.

IV. NONCONDENSABLE-GAS PUMPS

A. LHe Cryopump

Dewar-fed, finned-tube, LHe cryopumps are shielded by the moltrap elements. The lower section of each finned tube acts as a reservoir that is filled from an external helium Dewar. The boiling liquid supplies gas that maintains a gradient of 4 to 20°K. This arrangement avoids the temperature fluctuation problem inherent in gaseous supply systems. A carbon resistor, time-delay, liquid-level control system actuates the Dewar vent valve to maintain the reservoir level.

The 6,000-cm² projected area provides 50,000-liter/sec pumping speed for oxygen and nitrogen but requires only 2 liters of LHe per hour.

B. Ion Pump

It has been fairly well established that helium is pumped in ion pumps by first being ionized, the ions then striking the cathode with high enough energy to be buried in the surface. In the diode pump, the burial surface is continually bombarded by other high-energy ions which sputter titanium atoms off the surface. In doing so, some of the previously buried helium is released. In the triode pump, however, the collector surface is continually bombarded by fresh titanium, which aids in permanent burial of the already pumped helium. A diode pump typically pumps helium at about 10% of its rated speed for nitrogen, whereas the triode pump is typically 20% or over.

On the basis of superior helium pumping speed per unit pump inlet area, a triode configuration is selected which affords a speed of 0.7 liter/sec-in.²

Alnico-8 is selected as the magnet material because of its low loss of field strength when cooled to 100°K. From Parker and Studders (Ref. 2) it can be calculated that Alnico-8 would decrease 4% in field strength and that barium-ferrite would decrease 38% when cooled to 100°K.

One hundred General Electric 50-liter/sec (nitrogen) triode pump elements and encapsulated Alnico-8 magnets mounted between the molecular trap array and the inner liner provide 1000 liter/sec of helium pumping speed.

C. Titanium Sublimation Pump

The presently available commercial titanium sublimation pumps evaporate approximately 0.002 mole/hr of titanium. Clausing (Ref. 3) found that a mole ratio (titanium to pumped gas) of ten was required to achieve sticking factors of 0.15 for hydrogen and 0.55 for nitrogen gas. Thus in the case of hydrogen, the maximum quantity of gas that can be pumped by sublimation is

$$5.2 \times 10^{-4} \text{ torr-liter/sec.}$$

The unit surface area pumping speed is

$$3.86 \text{ liter/sec-cm}^2$$

where the volumetric flux rate has been calculated assuming the gas is at 100°K because of the low sticking fraction.

The moltrap array provides over 4×10^5 cm^2 of LN_2-cooled surface that is visible from the subpump located on the door, and this will provide a pumping speed of 1.5×10^6 liter/sec, or 1.5×10^{-4} torr-liter/sec for hydrogen. A standard 4-filament sublimation unit contains about 3.6 evaporable grams of titanium. This is sufficient material to operate for 60 hr at 10^{-10} torr.

The filaments are shielded so that titanium is not deposited upon the test item or the window.

Provision for mounting sublimators behind the molecular trap arrays have been made in case titanium does not have perfect capture upon LN_2-cooled surfaces.

It is conceivable that titanium sublimation onto the molecular trap arrays may also enhance the capture coefficient of the condensable molecules. It is known that the rebounding molecules accommodate with the surface and therefore have a finite residence time on the surface. If titanium is continuously coating the surface, then a portion of the rebounding molecules should be chemsorbed and thus permanently captured. If this proves to be the case, an electron-beam sublimator can replace the present filament unit and thus provide over 100 grams of titanium that can be evaporated continuously.

V. ROUGHING AND GUARD-VACUUM PUMPS

A. Mechanical Pump

A 270-cfm mechanical pump is used to rough-pump the 22,000-liter chamber to 0.1 torr in 20 min. The 6-in. roughing line is prevented from reaching transition flow conditions (0.1 torr) by a gaseous nitrogen leak, and thus backstreaming of pump oil is prevented.

B. Turbomol Pump

A 140-liter/sec turbomol pump is used to maintain 4×10^{-3} torr during a soft bake, to aid the LHe cryopump in the fine roughing of the chamber, and to maintain the guard vacuum at 3×10^{-5} torr. Backstreaming is prevented because the pressure ratio for high-molecular-weight molecules is very great. The high pumping speed for low-molecular-weight noncondensable gases complements the characteristics of the LHe cryopump.

C. LHe Cryopump

The high-vacuum LHe cryopump is used in conjunction with the turbomol pump to fine-rough pump the chamber from 0.1 to 1×10^{-6} torr.

VI. BAKE-OUT SYSTEM

A. Heater

In that the gravity-fed LN_2 system does not lend itself to forced hot gas circulation, nichrome ribbon electrical heaters are mounted on insulators on the inside of the inner liner. This arrangement supplies heat, by radiation, to the inner liner, the moltrap array, and the ion pump elements for bake-out.

B. Control

The 110-v, 500-amp ac power to the ribbon elements is controlled by a Leeds and Northrup Model "H" strip chart controller–recorder, which monitors any one of a number of copper–Constantan thermocouples mounted at strategic locations on the inner liner and moltrap array.

C. Hold-Down During Bake

Two different bake-out modes are required for the MOLSINK chamber. The first type, which will be termed a "hard" bake, is that which would be required for the initial chamber cleanup or after any prolonged exposure to atmospheric air or cleaning fluids. The second type of bake-out mode, termed a "soft" bake, will be the type used after the chamber has been brought up to atmospheric pressure with dry nitrogen and has not been exposed to atmospheric air. The hard bake is expected to require on the order of 100 hr while the soft bake should ordinarily be completed in a 1- to 10-hr period.

It will be assumed that in the case of the hard bake, all surfaces in the chamber will have an initial 300°K outgassing rate of 1×10^{-7} torr-liter/sec-cm^2.

For the soft bake, it is assumed that the surfaces are in a relatively clean condition initially, with an outgassing rate of 1×10^{-9} torr-liter/sec-cm^2.

The 125-liter/sec (270-cfm) mechanical roughing pump and a 140-liter/sec turbomol pump provide adequate pumping speed vs pressure over the range required. Larger turbomol pumps are available; however, very little is gained by going to larger pumps since changes by factors of two or three in the bake pressure will not materially affect the outgassing rate.

The pressures that can be maintained by each pump for the soft and hard bake are given in the following table and were calculated from Rogers (Ref. 4).

Type of pump	*Hard bake*	*Soft bake*
Mechanical	0.1 torr	0.1 torr
Turbomol	Cannot be used. (no speed at 0.1 torr)	4×10^{-3} torr

VII. CHAMBER

A. Support Structure

The inner liner is supported from the chamber's lower head and is removed by lowering it on the hydraulic lift. The inner liner supports carry the compressive-weight load of the inner liner and moltrap array assembly plus the tensile load applied by the 30-in. door-seal loading system.

The entire chamber is supported on four adjustable points attached to its cylindrical section. These points rest on the mid-point of four beams supported by four columns, which also serve as part of an overhead walking-beam crane structure. The crane and hydraulic door lift enable the chamber to be disassembled for major cleaning and maintenance.

B. Inner Liner

The inner liner is constructed of 304L stainless steel double-wall dimpled-plate. The upper end is a flat plate which separates at a metal-sealed bolted flange. The lower head contains the inner door flange, upon which the inner liner is supported.

The double wall is gravity fed from an integral LN_2 manifold, whose level is maintained by a pressure supply system.

The liner provides a vacuum-tight, LN_2-cooled wall between the test item and the warm outer chamber walls, elastomeric seals, and other contaminant sources.

C. Outer Chamber

The outer chamber provides the vacuum pressure vessel, supports the inner liner, and supports the door sealing loads. The ⅜-in.-thick 304L stainless-steel chamber has upper and lower 3:1 ellipsoidal ⅜-in.-thick heads, both of which are attached to the cylindrical section with O-ring-sealed, bolted flanges.

D. Double Door

The double door closes the outer chamber, acts as a high-vacuum valve between the test volume and the guard volume, and provides support points and feedthroughs for the test item.

1. Seal Design

The requirements of 250°C bake-out and LN_2 temperatures impose difficult demands on the 30-in.-diameter door seal. A temperature control system could be used with an elastomeric seal; however, this added complexity is undesirable. A Teflon gasket will withstand the temperature extremes but "flows" badly so that a continuous load must be applied to maintain the seal. The usual metal-to-metal shear-type gasket requires very high loading forces and would probably leak with thermal cycling. Fortunately, the seal design envisioned is between the guard vacuum and the inner chamber, so that the leakage problem is somewhat alleviated.

On the basis of the analysis by Armand, Lapujoulade, and Paigne (Ref. 5) of leakage between two metal surfaces in contact, a 2-in.-wide flange with a 30-in. inside diameter and with a 16-μ in. surface finish would result in a leak rate of 1.8×10^{-5} liter/sec between the guard vacuum and the test volume. It is assumed that long-wavelength distortions are eliminated through the application of 100 lb/in. of loading force on the flanges. With the guard vacuum at 1×10^{-6} torr, a leakage of ⅒ liter/sec can be tolerated without exceeding 1% of the high-vacuum pumping speed available in the test volume.

2. Door Lift

The hydraulic actuator mounted in a well in the floor raises and lowers the door, opens and closes the inner door, and is used to lower the lower head, inner liner, and moltrap array for cleaning and repair. The inner door closure is effected when the actuator compresses the springs that act to hold the two doors together.

E. Test Item Support

The model support consists of a catheter-fed, LN_2-cooled, sharp-knife-edge strut which provides overhead suspension points by which the test item may be hung by its own instrumentation wires. These wires are led up the back side of the strut and thus their contribution to the back reflection is minimized.

F. Window

The window is composed of an outer, optically flat, 1-in.-thick quartz plate, which withstands the atmospheric pressure, and an inner, optically flat, thin quartz plate, which separates the test volume from the guard vacuum. The inner window is an RCA type, which is sealed into a thin stainless-steel sleeve.

The inner window is shielded from the test item by a LN_2-cooled shutter that is supported on a magnetic rotary-motion feed-through. The shutter is provided with a molecular trap surface consisting of machined, circumferential, sharp V-grooves.

The outer window is sealed with a Viton Gask-O-Seal and is held in place by gravity, thus acting as an over-pressure relief for the chamber.

G. Burst Diaphragm

A 3-in. Fike double-dimpled, frangible-disk burst diaphragm provides external and internal over-pressure protection for the inner liner. Disk cutters are provided to insure that the diaphragm bursts at 1 psi differential pressure.

VIII. INSTRUMENTATION

A. Ion Gauge

A Varian Nude Ionization Gauge is mounted through the inner liner wall and monitors the test volume pressure between 1×10^{-4} torr and 1×10^{-11} torr. A Varian "Millitorr" Nude Ionization Gauge is mounted through the chamber wall and monitors the guard vacuum pressure between 1 torr and 5×10^{-6} torr.

B. Residual Gas Analyzer

A residual gas analyzer is mounted through the inner door and monitors the gases produced by the test item.

C. Titanium-Sublimation-Rate Monitor

A quartz-crystal microbalance mounted in the test volume is used to measure the rate at which titanium is deposited by the sublimation pumps.

D. LN_2-Cooled Quartz-Crystal Microbalance

A double quartz-crystal microbalance is mounted on a 77°K temperature-controlled support mounted on the moltrap array and is used to monitor the condensable molecular flux emanating from the test item. An identical crystal is mounted on the test item support and monitors the condensable molecular flux returning to the test item. These cryogenic quartz-crystal microbalances, arranged in this fashion, allow the molecular sink efficiency (N_r/N_s) to be continuously monitored.

E. LHe-Cooled Quartz-Crystal Microbalance

A double quartz-crystal microbalance is also mounted on the bottom of one of the helium cryopump elements and is used to monitor the rate at which gases are being cryopumped.

IX. DESCRIPTION OF MOLSINK OPERATION

The initial concept of operation of the MOLSINK facility is as follows:

1. All surfaces exposed to ultra-high vacuum are mechanically cleaned to remove titanium and contaminants deposited from previous tests.
2. The chamber is pumped down to 0.1 torr and baked out at 250°C for final removal of contaminants.
3. GN_2 is used to backfill the chamber and to maintain a continuous purge.
4. The test item is loaded into the chamber from the GN_2-purged plastic skirt area.
5. The chamber is mechanically pumped to 100 microns. Pressure is maintained in viscous flow with a GN_2 sweeping purge, which prevents the mechanical pump from backstreaming.
6. The moltrap shrouds and the inner liner are cooled to 77°K while the viscous-flow sweep purge is maintained.
7. The chamber is fine-rough pumped to 1×10^{-6} torr with the LHe cryopump and the turbomol pump.
8. The inner door is closed.
9. The guard vacuum is sustained with the turbomol pump.
10. The test volume is sustained with the LHe cryopump.
11. The He and H_2 are pumped with ion pumps operating at 77°K, in conjunction with titanium sublimation onto the moltrap shrouds.
12. The chamber is backfilled with GN_2.
13. The test item is unloaded into the GN_2-purged skirt area before the contaminants on the moltrap surfaces can evaporate.

GLOSSARY

Contaminant or condensable molecules. All molecules which at 300°K have a capture probability of 80% or greater on 100°K surface in a free-molecular-flow vacuum.

Glass-bead blasting. Glass beads (0.004 to 0.006 in. in diameter) are entrained in a jet of nitrogen gas (100 psi) and impelled against the surface to be cleaned. The cleaning action is due to the physical abrasion of the beads and their large, relatively clean, surface area. They are not toxic or explosive and do not leave a residue. Proper use of a bead blaster does not fracture the beads upon impact and thus microscopically peens the surface instead of cutting it.

Molecular trap ratio. The factor of molecular capture improvement of a molecular trap configuration over a smooth wall at the same effective distance from the test item.

Quartz-crystal microbalance. A quartz crystal vibrating in a thickness shear mode is sensitive to changes in mass on its surface; such changes produce a proportional shift in its resonant frequency that is readily measured. The frequency shift is proportional to the mass of material deposited and is independent of composition. This linear relationship prevails to within 1% for frequency shifts of 1% or less. A sensitivity of better than 1×10^{-8} gram/cm^2 is readily obtainable.

Test item diameter. The diameter of a theoretical, spherical test item. Actual spacecraft components have separated contaminant sources (electronic elements) and contaminant-sensitive surfaces (optical elements). The dimension of the contaminant source would correspond to the diameter of the theoretical test item. Thus, the major dimensions of items that could be effectively tested in the MOLSINK facility could exceed the specified 10-in. test-item diameter.

NOMENCLATURE

Symbols

A_c	area of cylinder bases on r_c and h
A_s	test item surface area
dA_1	elemental area
h	half height of moltrap array
L	depth of fin array
N_r	number of molecules returning to the test item
N_s	number of molecules emanating from test item
R	radius of test item
r_c	mean radius of moltrap array
r_t	radius of tangent sphere
W	width of fin array at entrance
Γ	recontamination coefficient
ε	bluntness fraction
ρ	open space fraction
σ	surface capture coefficient of array element surfaces

Abbreviations

MOLSINK	JPL's space molecular sink simulator
Moltrap array	molecular trap array
Subpump	titanium sublimation pump
Turbomol pump	Turbo-molecular impact pump

REFERENCES

1. Dawson, J. P., "Prediction of Cryopumping Speeds in Space Simulation Chambers," paper to be presented at the AIAA Space Simulation Testing Conference, Pasadena, Calif., November 1964.

2. Parker, R. J., and Studders, R. J., *Permanent Magnets and Their Application*, pp. 346–347, John Wiley and Sons, 1962.

3. Clausing, R. E., "Large-Scale Getter Pumping Experiment Using Vapor-Deposited Titanium Films," *Transactions of the American Vacuum Society*, p. 345, 1961.

4. Rogers, K. W., "The Variation in Outgassing Rate With the Time of Exposure and Pumping," *Transactions of the American Vacuum Society*, p. 84, 1963.

5. Armand, G., Lapujoulade, J., and Paigne, J., "A Theoretical and Experimental Relationship Between the Leakage of Gases Through the Interface of Two Metals in Contact and Their Superficial Micro-geometry," *Vacuum*, Vol. 14, No. 2, p. 53, February 1964.

6. Dawson, J. P., private communication, ARO, Inc., Tullahoma, Tenn.

APPENDIX A

Derivation of Contamination Equation for Idealized Spherical Case

The problem of determining the recontamination of a source sphere by an elemental area (dA_1) that is mounted at an angle η_0 to the radius extended from the sphere to the elemental area is essentially one of determining the form factor between the two surfaces. The molecular flux from the chamber walls which strikes the model and thus constitutes a contaminating influence is

$$N_w dA_1 F_{dA_1 - A_s}$$

The unit flux (N_w) leaving the wall is just the incoming flux times the fraction of the molecules that did not stick on first collision.

$$N_w = N_{in}(1 - \sigma)$$

Texts on radiative heat transfer give the following expression for the form factor.

$$F_{dA_1 - A_s} = \int_{A_s} \frac{\cos\eta \cos\theta}{\pi l^2} dA$$

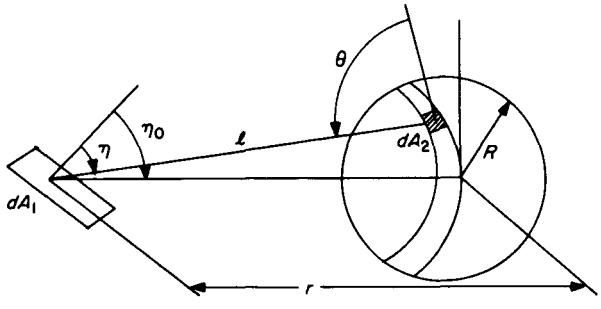

Integration yields the following equation if only one side of the area dA_1 is visible from the sphere.

$$F_{dA_1 - A_s} = \frac{dA_{1(\text{normal})}}{dA_1}\left(\frac{R}{r_c}\right)^2 = \cos\eta_0 \left(\frac{R}{r_c}\right)^2$$

The flux from the sphere to dA_1 can be obtained from the reciprocity theorem

$$dA_1 F_{dA_1 - A_s} = A_s F_{A_s - dA_1}$$

and the incoming flux becomes

$$N_{in} = N_s F_{dA_1 - A_s}$$

Then outgoing flux is

$$N_w = (1 - \sigma) N_{in} = N_s F_{dA_1 - A_s}(1 - \sigma)$$

Thus the flux returning to the sphere from the element is

$$N_w dA_1 F_{dA_1 - A_s} = N_s (1 - \sigma)\, dA_{1(\text{normal})} \cos\eta_0 \left(\frac{R}{r_c}\right)^4$$

Integration over the entire chamber surface gives the recontamination coefficient, i.e., the ratio of the returning molecules which strike the sphere to the emitted molecules.

$$\Gamma = (1 - \sigma)\cos\eta_0 \left(\frac{R}{r_c}\right)^2$$

This can also be related to a tangent sphere, not necessarily the source sphere size but in effect a maximum model size for a particular value of the trap element angle chosen, η_0, because of the limitation in the derivation to flux from only one side of the elemental area, dA_1.

$$\Gamma = (1 - \sigma)\frac{r_t}{r_c}\left(\frac{R}{r_c}\right)^2$$

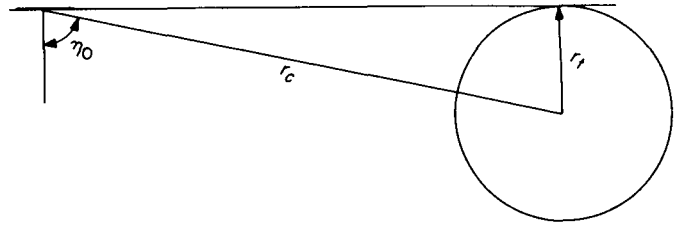

APPENDIX B

Sticking Coefficient

The values of the sticking coefficient, σ, for water vapor condensing on LN_2-cooled surfaces as reported in the literature show some variations, but recent data from Dawson (Ref. 6) indicate values of 0.85 to 0.9 for 300°K water vapor. Dawson (Ref. 1) suggests that the variation of the sticking coefficient with temperature can be approximated by the following relationship:

$$(1 - \sigma)^T = (1 - \sigma_0)^{T_0}$$

The source gas in the MOLSINK is assumed to be water vapor at 400°K. Using an average value of $\sigma_0 = 0.88$ at 300°K and the above temperature relationship,

$$\sigma_{400°K} = 0.80$$

APPENDIX C

Contamination Coefficient in Idealized Case for a Specific Sticking Coefficient

The use of the idealized solution of Appendix A and the sticking coefficient of Appendix B will yield an idealized contamination coefficient.

The value of η_0 chosen in the design is a result of a trade-off study between panel fabrication cost, chamber shell cost, and the general level of recontamination desired. The final design value is $\eta_0 = 6°40'$ at an array mean radius of 43 in. The tangent sphere radius r_t is then equal to 5 in.

The contamination coefficient for this configuration if the source sphere is 10 in. in diameter is

$$\Gamma = (1 - \sigma)\frac{r_t}{r_c}\left(\frac{R}{r_c}\right)^2 = (0.2)\left(\frac{5}{43}\right)\left(\frac{5}{43}\right)^2 = 3.16 \times 10^{-4}$$

APPENDIX D

Cylindrical Molecular Sink

The fabrication of a spherical molecular sink array, although possible, presents many fabrication problems that are considerably alleviated when a cylindrical array is used.

A. Vertical Fin Recontamination

The recontamination rate for a vertical fin with its surface normal to a radius line at the midpoint is

$$N = 2N_s(1-\sigma)\,dy\int_0^h \left(\frac{R}{r}\right)^4 \cos^2\gamma\,dz$$

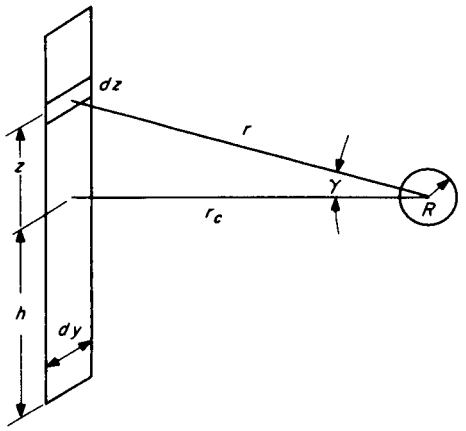

Integration over the fin height gives

$$N = N_s(1-\sigma)\,dy\,\frac{r_c}{2}\left(\frac{R}{r_c}\right)^4\left\{\frac{\frac{h}{r_c}}{\left[\left(\frac{h}{r_c}\right)^2+1\right]^2} + \frac{3}{2}\left[\frac{\frac{h}{r_c}}{\left(\frac{h}{r_c}\right)^2+1} + \tan^{-1}\frac{h}{r_c}\right]\right\}$$

Now if the fin is rotated by angle η_0 to the radial line, a new expression is found for the recontamination rate.

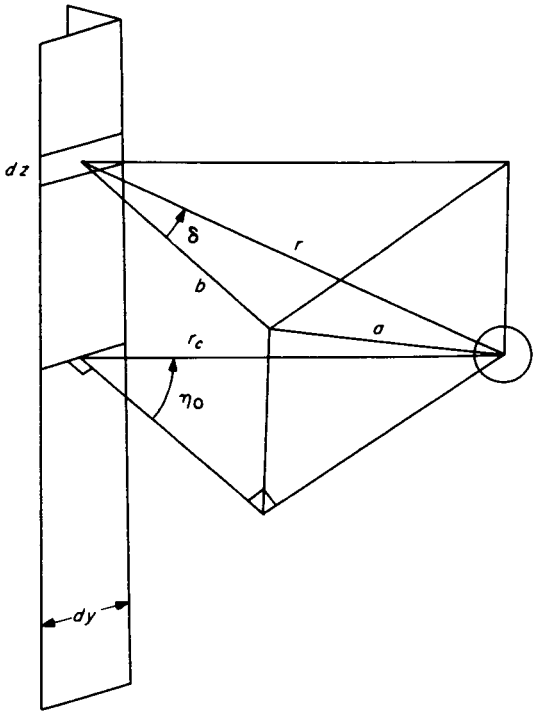

$$N = 2N_s(1-\sigma)\,dy\int_0^h \left(\frac{R}{r}\right)^4 \cos^2\delta\,dz$$

$$\cos\delta = \frac{\cos^2\eta_0}{1+\left(\frac{Z}{r_c}\right)^2}$$

Therefore

$$N = N_s(1-\sigma)\,dy\,r_c\left(\frac{R}{r_c}\right)^4\frac{\cos^2\eta_0}{2}\left\{\frac{\frac{h}{r_c}}{\left[\left(\frac{h}{r_c}\right)^2+1\right]^2} + \frac{3}{2}\left[\frac{\frac{h}{r_c}}{1+\left(\frac{h}{r_c}\right)^2} + \tan^{-1}\frac{h}{r_c}\right]\right\}$$

B. End Disc Recontamination

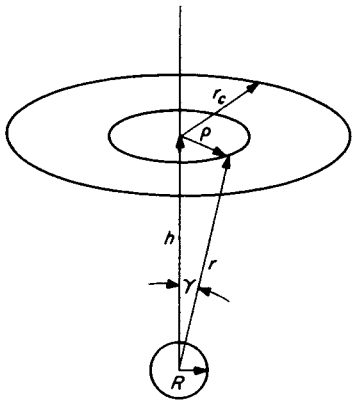

The normal end disc recontamination rate is

$$N = N_s(1-\sigma)\int_0^{r_c} 2\pi\rho\cos^2\gamma\left(\frac{R}{r}\right)^4 d\rho$$

Integration yields

$$N = N_s(1-\sigma)\frac{\pi r_c^2}{2}\left(\frac{R}{r_c}\right)^4 \frac{\left[\left(\frac{h}{r_c}\right)^2+1\right]^2-\left(\frac{h}{r_c}\right)^4}{\left(\frac{h}{r_c}\right)^2\left[\left(\frac{h}{r_c}\right)^2+1\right]}$$

If the disc makes an angle η_0 with h, the expression becomes

$$N = N_s(1-\sigma)\frac{\pi r_c^2}{2}\left(\frac{R}{r_c}\right)^4\cos\eta_0 \frac{\left[\left(\frac{h}{r_c}\right)^2+1\right]^2-\left(\frac{h}{r_c}\right)^4}{\left(\frac{h}{r_c}\right)^2\left[\left(\frac{h}{r_c}\right)^2+1\right]}$$

C. Closed Cylindrical Array

Summing the cylinder and end recontamination rates and expressing the result in terms of recontamination coefficient gives

$$\Gamma = (1-\sigma)\cos\eta_0\left(\frac{R}{r_c}\right)^2\Phi$$

where

$$\Phi = \frac{1}{4}\left\{\frac{\left[1+\left(\frac{h}{r_c}\right)^2\right]^2-\left(\frac{h}{r_c}\right)^4}{\left(\frac{h}{r_c}\right)^2\left[1+\left(\frac{h}{r_c}\right)^2\right]^2} + \frac{3}{2}\left[\frac{\frac{h}{r_c}}{1+\left(\frac{h}{r_c}\right)} + \tan^{-1}\left(\frac{h}{r_c}\right)\right] + \frac{\frac{h}{r_c}}{\left[1+\left(\frac{h}{r_c}\right)^2\right]^2}\right\}$$

Expressing R/r_c in terms of A_c/A_s and h/r_c gives

$$\Gamma = (1-\sigma)\cos\eta_0\frac{A_s}{A_c}\left(\frac{h}{r_c}+\frac{1}{2}\right)\Phi$$

Examination of the function

$$\frac{\Gamma\frac{A_c}{A_s}}{(1-\sigma)\cos\eta_0}$$

reveals the fact that a minimum exists near $h/r_c = 0.9$ although the recontamination in general is not a strong function of h/r_c between h/r_c equal to 0.8 to 1.0.

Using this optimum value of h/r_c, the recontamination coefficient can be found for an optimum cylindrical array which has the same cylinder diameter as the spherical array discussed in Appendix C.

$$\Gamma = (1-\sigma)\cos\eta_0\frac{A_s}{A_c}\left(\frac{h}{r_c}+\frac{1}{2}\right)\Phi$$

where

$$\left(\frac{h}{r_c}+\frac{1}{2}\right)\Phi = 1.09$$

$$R = 5\text{ in.}$$

$$r_c = 43\text{ in.}$$

$$\cos\eta_0 = 0.1161$$

The value of h/r_c actually used in the final design is $h/r_c = 0.815$ and, therefore,

$$\left(\frac{h}{r_c}+\frac{1}{2}\right)\Phi = 1.095$$

and thus

$$\Gamma_{\text{cylinder}} = 2.62\times10^{-4}$$

APPENDIX E

Composite Array Recontamination Rate

In the present design, a combination of cylindrical and spherical sections has been chosen to best fit the various needs envisioned for ease of maintenance and cleaning in the chamber. The arrays are essentially divided along the midpoint into these two configurations and thus the composite recontamination should be the sum of one-half the recontamination coefficients for the spherical and the cylindrical solutions. In the design, the mean sphere array radius is 41 in., while the cylinder radius is 43 in.

$$\Gamma_{\text{composite}} = \frac{\Gamma}{2}\bigg|_{\text{sphere}} + \frac{\Gamma}{2}\bigg|_{\text{cylinder}}$$

$$= \frac{3.64 \times 10^{-4}}{2} + \frac{2.62 \times 10^{-4}}{2}$$

$$= 3.13 \times 10^{-4}$$

APPENDIX F

Effect of Distributed Bluntness

A compromise must be made, when designing a molecular sink array, between minimizing the normal areas in the array, i.e., the leading edge and root sharpness, and the cost of fabrication. It therefore is important to evaluate the effect of distributed bluntness on the recontamination coefficient.

If ε is the fraction of the surface area which is uniformly distributed normal surface area, then the recontamination coefficient for the cylindrical array can be expressed as

$$\Gamma_{cy} = (1 - \sigma)\,[\varepsilon + (1 - \varepsilon)\cos\eta_0]\frac{A_s}{A_c}\Phi\left(\frac{h}{r_c} + \frac{1}{2}\right)$$

The array is fabricated of 0.02-in.-thick copper sheet, which is rolled at the leading edge to give a 0.04-in.-wide end. This leading edge is, of course, actually a curved surface; however, it will be considered to be normal area in this contamination determination. The spacing between leading edges is 2 in., and therefore,

$$\varepsilon = \frac{0.04}{2} = 0.02$$

and the recontamination coefficient for a cylindrical array with this distributed bluntness becomes

$$\Gamma_{cy} = 0.2\,[0.02 + (0.98)\,(0.1161)]\,(0.0103)\,(1.095)$$

$$= 3.02 \times 10^{-4}$$

For the spherical case

$$\Gamma_s = (1 - \sigma)\,[\varepsilon + (1 - \varepsilon)\cos\eta_0]\left(\frac{R}{r_c}\right)^2$$

$$\Gamma_s = 3.9 \times 10^{-4}$$

and for the composite case with bluntness

$$\Gamma = \frac{3.02 \times 10^{-4}}{2} + \frac{3.9 \times 10^{-4}}{2} = 3.46 \times 10^{-4}$$

APPENDIX G

Effect of Finite Fin Depth

Consideration of the molecular sink array surfaces as incremental areas is convenient as an analytical technique. However, as the arrays become a significant fraction of the chamber radius, nonuniform flux distribution will produce deviations from the incremental results.

Considering the angle fin in the following sketch, the recontamination is given by

$$N = N_s(1-\sigma)\int_A (F_{dA_1-A_s})^2\, dA_1$$

$$= N_s(1-\sigma)\, dz \int_0^l \cos^2\eta \left(\frac{R}{r'}\right)^4 d\xi$$

where

$$\cos\eta = \frac{a}{r'} \qquad r'^2 = a^2 + (\xi_0 + \xi)^2$$

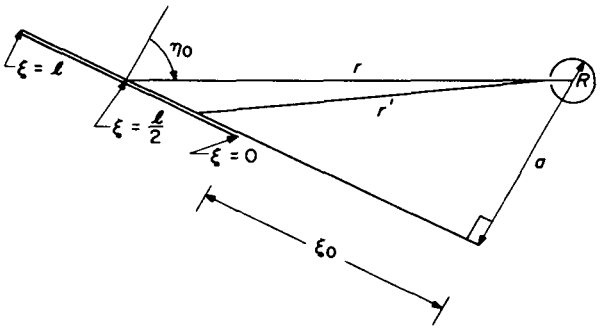

The recontamination becomes

$$N = N_s(1-\sigma)\, dz \left(\frac{R}{a}\right)^4 a \int_{\xi_0/a}^{(\xi_0+l)/a} \frac{d\left(\frac{\xi_0+\xi}{a}\right)}{\left[1+\left(\frac{\xi_0+\xi}{a}\right)^2\right]^3}$$

Integrating,

$$N = N_s(1-\sigma)\, dz \left(\frac{R}{a}\right)^4 \frac{a}{4}\left\{\frac{\psi(1+\Lambda)}{\psi^2(1+\Lambda)^2+1} - \frac{\psi}{\psi^2+1^2}\right.$$

$$+ \frac{3}{2}\left[\frac{\psi(1+\Lambda)}{\psi^2(1+\Lambda)^2+1} - \frac{\psi}{\psi^2+1}\right.$$

$$\left.\left. + \tan^{-1}\frac{\psi\Lambda}{1+\psi^2(1+\Lambda)}\right]\right\}$$

where

$$\psi = \frac{\xi_0}{a}, \qquad \Lambda = \frac{l}{\xi_0}$$

For the range of fin geometry of interest in this analysis, it was found that the solution for a radial-fin array and the wedge-fin array were very similar and, since the radial-fin solution is much simpler, it has been used to give a better insight into the relative importance of the finite depth. When the resultant recontamination rate is ratioed to the recontamination rate per unit fin area of an elemental area located at the center of the fin, the following expression is obtained

$$\frac{\Gamma_{\text{finite}}}{\Gamma_{\text{elemental}}} = \left(\frac{r_c}{r_0 - r_i}\right)\left\{\frac{\frac{1}{5}\left[\left(\frac{1}{1-\left(\frac{r_0-r_i}{2r_c}\right)}\right)^5 - \left(\frac{1}{1+\left(\frac{r_0-r_i}{2r_c}\right)}\right)^5\right] + \frac{3}{35}\left(\frac{R}{r_c}\right)^2\left[\left(\frac{r_c}{r_i}\right)^7 - \left(\frac{r_c}{r_0}\right)^7\right]}{1+\frac{3}{5}\left(\frac{R}{r_c}\right)^2}\right\}$$

For most cases,

$$\left(\frac{R}{r_c}\right)^2 << 1$$

and the equation can be simplified to the following:

$$\frac{\Gamma_{\text{finite}}}{\Gamma_{\text{elemental}}} = \left(\frac{r_c}{r_0 - r_i}\right)\frac{1}{5}\left\{\left[\frac{1}{1-\left(\frac{r_0-r_i}{2r_c}\right)}\right]^5 - \left[\frac{1}{1+\left(\frac{r_0-r_i}{2r_c}\right)}\right]^5\right\}$$

For a cylinder, then, the percentage of increase in recontamination for the finite fin effect is $\Delta\Gamma/\Gamma = 0.082$, for $r_0 - r_i = 10$ in., $r_c = 43$ in. For a sphere, $\Delta\Gamma/\Gamma = 0.05$, for $r_0 - r_i = 7.5$ in., $r_i = 41$ in. Thus a composite array with finite fin depth has the following recontamination coefficient:

$$\Gamma = 3.33 \times 10^{-4}$$

If distributed bluntness is included,

$$\Gamma = 3.68 \times 10^{-4}$$

APPENDIX H

Effect of Open Space Between Arrays

Despite care in fabrication and assembly of the molecular sink arrays, or because of slight warpage during thermal cycling, there will undoubtedly be a certain amount of open space between the leading edges of adjacent arrays. The following analysis is an assessment of the recontamination due to these spaces:

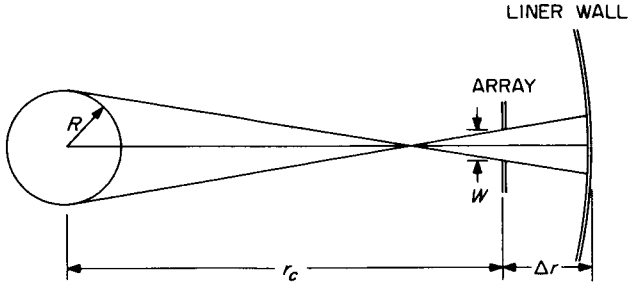

$$\beta = \frac{\Sigma W}{2r_0} = \begin{array}{l}\text{fraction of the normal array}\\ \text{surface with open space}\end{array}$$

Then the recontamination coefficient, from the open space only, becomes

$$\Gamma_{os} = \beta\left(\frac{R}{r_c}\right)^2(1-\sigma)\left(\frac{h}{r_c}+\frac{1}{2}\right)\Phi\left[\frac{1}{\left(1+\frac{\Delta r}{r_0}\right)\left(1+\frac{R}{r_0}\frac{2\Delta r}{W}\right)}\right]$$

Thus the fractional increase in recontamination due to the open spaces is

$$\frac{\Delta\Gamma}{\Gamma} = \beta\left[\frac{1}{\left(1+\frac{\Delta r}{r_0}\right)\left(1+\frac{R}{r_0}\frac{2\Delta r}{W}\right)\cos\eta_0} - 1\right]$$

Since it is impossible to predict accurately the amount of open space that will exist when the arrays are assembled, a conservative example will be used to indicate the degree of seriousness of the effect. The most adverse case occurs when the back reflecting wall is close to the array opening. This case will be examined with an assumed gap opening of ⅛ in. at every array and a gap-to-wall distance of 2½ in.

$$\Delta r = 2.5 \text{ in.}$$

$$r_0 = 48 \text{ in.}$$

$$W = 0.125 \text{ in.}$$

$$\beta = \frac{(60)(0.125)}{2(48)} = 0.078$$

$$\frac{\Delta\Gamma}{\Gamma} = 0.078\left[\frac{1}{\left(1+\frac{2.5}{48}\right)\left[1+\left(\frac{5}{48}\right)\frac{5}{0.125}\right]0.1161} - 1\right]$$

$$= 0.0453$$

Only a 4½% increase in contamination would thus result from this conservative example. If, in fact, this open-space condition did exist in addition to the other factors mentioned in Appendixes E, F, and G, the total recontamination coefficient would become

$$\Gamma = 3.86 \times 10^{-4}$$

APPENDIX I

Effect of Multiple Wall Collisions

In order to estimate the number of molecules that return to the test item sphere after multiple collisions with the wall, it is necessary to estimate the sticking coefficient for second and succeeding collisions. This sticking coefficient may differ from the value for the first collision, since the rebounding molecule will be at a lower temperature. From the results of Dawson (Ref. 1), reducing the gas temperature will significantly increase the sticking coefficient, and since the sticking coefficient for room temperature water vapor is already in the range of 0.85 to 0.9, it appears that there is little likelihood of any measurable fraction of the molecules returning after the second collision unless the accommodation coefficient is very low. Although accommodation coefficient data are not available on condensate-covered surfaces, a conservative estimate of the effect can be made by assuming a coefficient of 0.9, which is common for engineering surfaces. This gives second-collision molecules a sticking coefficient of $\sigma_x = 0.993$. The percentage increase in recontamination coefficients due to second collisions is

$$\frac{\Delta\Gamma}{\Gamma} = \frac{(1-\sigma_{400}) + (1-\sigma_{400}) - \sigma_x(1-\sigma_{400}) - (1-\sigma_{400})}{1-\sigma_{400}}$$

$$= (1-\sigma_x) = 0.007$$

The total recontamination coefficient, including all of the effects analyzed in Appendixes E, F, G, H, and I, is then

$$\Gamma_{total} = 3.89 \times 10^{-4}$$